Biochemical and Biophysical Research Communications 443 (2014) 518–523

Contents lists available at ScienceDirect

Biochemical and Biophysical Research Communications

journal homepage: www.elsevier.com/locate/ybbrc

The multiple expression of Ca^{2+}-activated Cl^- channels via homo- and hetero-dimer formation of TMEM16A splicing variants in murine portal vein

Junya Ohshiro, Hisao Yamamura, Takanori Saeki, Yoshiaki Suzuki, Yuji Imaizumi *

Department of Molecular and Cellular Pharmacology, Graduate School of Pharmaceutical Sciences, Nagoya City University, Nagoya 467-8603, Japan

ARTICLE INFO

Article history:
Received 22 November 2013
Available online 7 December 2013

Keywords:
TMEM16A
Ca^{2+}-activated Cl^- channel
Vascular smooth muscle
Splicing variants
Single molecular imaging

ABSTRACT

Ca^{2+}-activated Cl^- channel (CaCC) often plays substantial roles in the regulation of membrane excitability in smooth muscle cells (SMCs). TMEM16A, a member of the TMEM16 family, has been suggested as the molecular entity responsible for CaCC in several types of SMCs. In this study, the expression of TMEM16A splicing variants and their contribution to CaCC activity were examined in murine portal vein SMCs (mPVSMCs). Four transcripts of TMEM16A splicing variants, which include four alternatively spliced segments ("*a*" and "*b*" in N-terminus and "*c*" and "*d*" in the first intracellular loop), were identified; the expression ratio of four transcripts of "*abc*", "*acd*", "*abcd*" and "*ac*" was 64.5, 25.8, 4.8 and 4.8%, respectively. The immunostaining of isolated mPVSMCs with anti-TMEM16A antibody indicates the abundant expression of TMEM16A on the cell membrane. CaCC currents recorded in mPVSMCs were markedly reduced by $T16A_{inh}$-A01, a specific TMEM16A inhibitor. When the two major TMEM16A splicing variants, *abc* and *acd* isoforms, were expressed separately in HEK293 cells, the CaCC currents, which possess similar electrophysiological characteristics to those in mPVSMCs were observed. The single-molecule photobleaching analyses using total internal reflection fluorescence (TIRF) microscope indicated that the distribution of stepwise photobleaching events was fit well with a binomial distribution for homodimer. Additionally, the heterodimer formation was suggested by fluorescence resonance energy transfer (FRET) analyses in HEK293 cells co-expressing CFP- or YFP-tagged variants. In conclusion, alternatively spliced variants of TMEM16A *abc* and *acd* in mPVSMCs are two major molecular entities of CaCC and may form hetero-/homo-dimers to be functional as CaCC in the regulation of membrane excitability and contractility in mPVSMCs.

1. Introduction

Ca^{2+}-activated Cl^- channels (CaCCs) are expressed ubiquitously in various types of cells and play wide variety of physiological roles including fluid secretion, neuronal excitation, and smooth muscle (SM) contraction. Particularly in vascular SM cells (SMCs), the activation of CaCC contributes to the shift of resting membrane potential to positive direction and regulates Ca^{2+} influx through voltage-dependent Ca^{2+} channels, resulting in the increase in muscle tone in several arteries and veins [1]. Portal vein shows spontaneous contractions, which substantially contribute to the blood flow from mesenteric vascular beds to liver and the application of CaCC blockers markedly reduces the portal vein contractions [2]. Therefore, the identification of molecular entity of CaCC in portal vein, is one of the emergent issues for obtaining the comprehensive understanding of mechanisms underlying the physiological and pathophysiological regulations of gastro-liver circulation.

Recently, TMEM16A and TMEM16B, which belong to TMEM16 family, have been identified as the counterpart of classic CaCC [3–5]. TMEM16A is expressed in various tissues including vascular SMs and expected to regulate their functions [6–8]. The pharmacological blockade of TMEM16A leads to muscle relaxation in thoracic aorta and mesenteric artery [9]. TMEM16A has eight putative transmembrane domains and is presumed to form dimers as a functional CaCC [10,11]. In addition, TMEM16A has at least four alternatively spliced segments (named segments: *a*, *b*, *c*, and *d*). The inclusion or skipping of these segments alters electrophysiological properties of TMEM16A CaCC activity, while the details have not been elucidated yet. The segment *b* includes putative calmodulin binding domain and segment *c* affects voltage dependence [12,13]. Moreover, skipping of segment *d* changes activation kinetics [14]. Thus, TMEM16A can produce multiple protein isoforms and may differentially contribute to CaCC activity.

* Corresponding author. Address: Department of Molecular and Cellular Pharmacology, Graduate School of Pharmaceutical Sciences, Nagoya City University, 3-1 Tanabedori Mizuhoku, Nagoya 467-8603, Japan. Fax: +81 52 836 3431.
E-mail address: yimaizum@phar.nagoya-cu.ac.jp (Y. Imaizumi).

0006-291X/$ - see front matter © 2013 Elsevier Inc. All rights reserved.
http://dx.doi.org/10.1016/j.bbrc.2013.11.117

However, the proportional expression of each TMEM16A splicing variant and the interaction between different variants have been totally unknown regardless of cell types.

The present study was undertaken to elucidate the molecular entities of CaCC in murine portal vein smooth muscle cells (mPVSMCs). We found that TMEM16A splicing variants were expressed and substantially responsible for CaCC activity in mPVSMCs. Results suggest that the mixed expression of homodimers and heterodimers may determine the features of CaCC activity in mPVSMCs.

2. Materials and methods

2.1. Cell isolation

All experiments were approved by the Ethics Committee of Nagoya City University and were conducted in accordance with the Guide for the Care and Use of Laboratory Animals of the Japanese Pharmacological Society. The portal veins were dissected from male mice (C57BL/6, 8–12 weeks; Japan SLC, Hamamatsu, Japan) and incubated in Ca^{2+}/Mg^{2+}-free Hanks solution for 10 min at 37 °C. Then, the tissues were incubated in Ca^{2+}/Mg^{2+}-free Hanks solution containing 0.3% collagenase type IA, 0.2% trypsin inhibitor, 0.2% bovine serum albumin, and 0.01% protease type XIV (Sigma–Aldrich, St. Louis, USA) for 10 min at 37 °C. After incubation, myocytes were isolated by gentle agitation with a glass pipette.

2.2. Cell culture

HEK293 cells were obtained from the Health Science Research Resources Bank (Osaka, Japan) and cultured in Dulbecco's Modified Eagle's Medium (DMEM) supplemented with 10% fetal bovine serum (FBS), 20 U/ml penicillin, and 20 μg/ml streptomycin (Sigma–Aldrich) at 37 °C.

2.3. Plasmid constructs

The cDNAs encoding mouse TMEM16A spliced variants were cloned from portal veins and subcloned into pcDNA3.1(+) (Invitrogen, Carlsbad, USA), pEYFP-N1, pECFP-N1, and pEGFP-N1 (Clontech Laboratories, Mountain View, USA). HEK293 cells were transiently transfected with cDNA using LipofectAmine 2000 (Invitrogen). Experiments were preformed 24–72 h after transfection.

2.4. Electrophysiological recordings

Electrophysiological studies were performed using a whole cell voltage-clamp technique with an EPC-7 amplifier (HEKA Electronics, Darmstadt, Germany), an analog–digital converter (Digidata 1440A), and pCLAMP software (version 10.2; Axon Instruments, Foster City, USA), as described previously [15,16].

2.5. RT-PCR and real-time PCR

Total RNA was extracted from murine portal veins and used for reverse transcription (RT). Following PCR primer set was used for spliced variant analysis of mouse TMEM16A (GenBank Accession No. NM_178642): (+) 5′-ATG CAG GAC GCG CAG GAC AGC GA-3′ and (−) 5′-AAG ATG ATG GAG ACA AGA TTG GT-3′. Quantitative real-time PCR analysis was performed using the SYBR Green assay (SYBR Premix Ex Taq; Takara Bio, Otsu, Japan) on an ABI PRISM 7000 sequence detection system (Applied Biosystems, Foster City, USA). Specific PCR primers were designed as follows: mouse TMEM16A (NM_178642, 2649–2781), TMEM16B (BC033409, 2374–2494), TMEM16C (NM_001128103, 2575–2686), TMEM16D (NM_178773, 2109–2221), TMEM16E (NM_177694, 2286–2386), TMEM16F (NM_175344, 2388–2493), TMEM16G (NM_207031, 2179–2283), TMEM16H (NM_001164679, 2221–2328), TMEM16J (NM_178381, 2009–2112), TMEM16K (NM_133979, 1601–1702), and GAPDH (NM_008084, 730–833).

2.6. Immunocytochemistry

Immunocytochemical experiment was performed using anti-TMEM16A antibody (ab16293, 1:50 dilution, Abcam, Cambridge, USA) and Alexa Fluor 488 anti-chicken IgG (A11039, 1:1000 dilution, Molecular Probes, Eugene, USA) [15]. Confocal images were obtained using a laser scanning confocal fluorescent microscope (A1R) equipped with a fluorescent microscope (ECLIPSE Ti), an objective lens (Plan Apo 60× 1.40 NA, oil immersion) and NIS Elements software (version 3.10; Nikon, Tokyo, Japan).

2.7. TIRF imaging and FRET analysis

Single-molecule imaging was performed with total internal reflection fluorescence (TIRF) imaging system, which consisted of a fluorescent microscope (ECLIPSE TE2000-U; Nikon), an objective lens (CFI Apo TIRF 60×/1.45, oil immersion; Nikon), an EM-CCD camera (C9100-12; Hamamatsu Photonics, Hamamatsu, Japan), and AQUACOSMOS software (version 2.6; Hamamatsu Photonics) [15]. The resolution of images was 178 nm/pixel (x–y). Efficiency of fluorescence resonance energy transfer (FRET) was evaluated based on the acceptor photobleaching method, as previously reported [15]. The fluorescence of YFP was photobleached for 2 min. TIRF images were acquired for 4650 ms. FRET efficiency (E_{FRET}) was calculated using the following equation: E_{FRET} (%) = $[(CFP_{after} - CFP_{before})/CFP_{after}] \times 100$, where CFP_{after} and CFP_{before} are CFP emissions after and before YFP photobleaching, respectively.

2.8. Single-molecule GFP bleaching

The oligomerization of TMEM16A was examined by the single-molecule photobleaching method [15,17]. TMEM16A-trasnfected HEK293 cells were fixed with 4% paraformaldehyde in phosphate buffered saline (PBS) for 10 min. TIRF images with the resolution of 178 nm/pixel were scanned every 100 ms. Fluorescent intensity in a region of interest (ROI, 3 × 3 pixels) was calculated by subtracting the background in 16 pixels around the ROI.

2.9. Solutions

Ca^{2+}/Mg^{2+}-free Hanks solution contained (in mM) 137 NaCl, 5.4 KCl, 0.17 Na_2HPO_4, 0.44 KH_2PO_4, 4.2 $NaHCO_3$, and 5.6 glucose. For electrophysiological recordings, the bath solution contained (in mM) 137 NaCl, 5.9 KCl, 2.2 $CaCl_2$, 1.2 $MgCl_2$, 14 glucose, 20 TEA-Cl, and 10 HEPES. The pH was adjusted to 7.4 with NaOH. The pipette solution contained (in mM) 120 CsCl, 20 TEA-Cl, 2.8 $MgCl_2$, 10 HEPES, 2 $ATPNa_2$, 5 EGTA, and 4.25 $CaCl_2$ (pCa 6.0). The pH was adjusted to 7.2 with CsOH.

2.10. Chemicals

Pharmacological reagents were obtained from Sigma–Aldrich except for $T16A_{inh}$-A01 (Tocris Bioscience, Bristol, UK). $T16A_{inh}$-A01 was dissolved in dimethyl sulfoxide at the concentration of 10 mM as a stock solution.

2.11. Statistics

Data are expressed as mean ± SE. Statistical significance between two groups was determined using Student's t-test.

Statistical significance between among groups was evaluated by Tukey's test. P values < 0.05 were considered statistically significant.

3. Results and discussion

3.1. Several members of TMEM16 family are expressed in portal vein

Several molecules have been proposed as candidates responsible for CaCC. It has been shown that mCLCA1 is expressed and may contribute to CaCC activity in mPVSMCs [18]. In addition, Best3, which belongs to bestrophin family, has been reported to be expressed in several vascular SMCs (VSMCs) and essential for cGMP-dependent CaCC activity [19]. To examine the expression of TMEM16 family in mPVSMCs, we took the real-time quantitative PCR approach. Fig. 1A demonstrates that mRNAs for TMEM16A, TMEM16F, and TMEM16K were substantially expressed in murine portal vein, while transcripts of TMEM16B-E, TMEM16G-H, and TMEM16J were expressed at low levels (TMEM16A: 0.027 ± 0.006, TMEM16F: 0.018 ± 0.005, TMEM16K: 0.036 ± 0.008, n = 3). Immunocytochemical imaging showed that TMEM16A protein was abundantly expressed on plasma membrane of mPVSMCs (Fig. 1B).

These gene expression patterns are similar to those reported in some VSMCs [20,21]. In contrast to TMEM16A and TMEM16B, other members of TMEM16 family are considered to be not ion channels responsible for CaCC. The electrophysiological properties of TMEM16F have remained controversial: small conductance Ca^{2+} activated nonselective cation (SCAN) channel [22] and outward rectifying Cl^- channel [23]. As for CaCC activity, TMEM16F activation requires high concentration of intracellular free Ca^{2+} compared with TMEM16A [24,25]. Under the experimental conditions in this study, TMEM16F may make little contribution, if any, to CaCC activity in mPVSMCs. Because of the strong contraction of the myocytes, membrane currents could not be measured using the pipette solution with concentrations of Ca^{2+} higher than 1 μM Ca^{2+}.

3.2. TMEM16A contributes to CaCC current in mPVSMCs

CaCC currents were measured under whole-cell patch clamp configuration, using the pipette solution contained 120 mM CsCl, 20 mM TEA-Cl and 1 μM Ca^{2+}. The outward currents and tail currents with slow activation and deactivation kinetics, respectively, were measured upon depolarization from holding potential of −60 mV (Fig. 2A). The tail currents were detected at the −60 mV. The shapes of the currents are similar to those of CaCC previously reported in several visceral SMCs [2,6,8,9,18] The current–voltage relationship denotes the substantial outward current density and the outward rectification (at 120 mV: 36.4 ± 5.8 pA/pF, n = 3; Fig. 2C). The application of 100 μM niflumic acid significantly reduced both the outward CaCC currents and tail currents (Fig. 2Ba). The relative peak amplitude of outward currents at +100 mV and the inward tail currents at +100 mV were inhibited to 0.30 ± 0.04 (n = 6, P < 0.01) and 0.35 ± 0.04 (P < 0.01) in the presence of 100 μM niflumic acid, respectively, when the amplitude before the application was taken as unity (1.0) (Fig. 2Bb and Db). $T16A_{inh}$-A01 is a blocker more selective to TMEM16A on the voltage-independent block mechanism [26]. The application of 10 and 30 μM $T16A_{inh}$-A01 reduced the peak outward current to 0.53 ± 0.03 (n = 9, P < 0.01) and to 0.38 ± 0.01 (n = 3, P < 0.01), respectively (Fig. 2Db). The tail currents were also reduced to 0.55 ± 0.03 (P < 0.01) and to 0.36 ± 0.01 (P < 0.01), respectively, as has been reported in pulmonary artery SMCs [8].

Although $T16A_{inh}$-A01 inhibits TMEM16B as well as TMEM16A [26], the expression of TMEM16B transcripts was much lower than that of TMEM16A. The immunocytochemical staining of mPVSMCs with anti-TMEM16B antibody (ab91573, 1:100 dilution, Abcam) denoted no clear signals on cell membrane (unpublished observation). In addition, the activation and deactivation kinetics of CaCC in mPVSMCs were much slower than those reported on TMEM16B [27]. Taken together, results strongly suggest that the large part of CaCC current, maybe at least ~70%, in mPVSMCs was caused by TMEM16A activation.

3.3. Two splicing variants of TMEM16A are mainly expressed in mPVSMCs

It has been suggested that TMEM16A generates multiple protein isoforms by the combination of spliced segments *a–d* (Fig. 3Aa) [3,12]. To identify TMEM16A splicing variants, which are expressed in mPVSMCs, we designed a primer pair spanning the exons encoding the segment *a–d* and performed RT-PCR analyses. The murine portal vein cDNA products were amplified, and

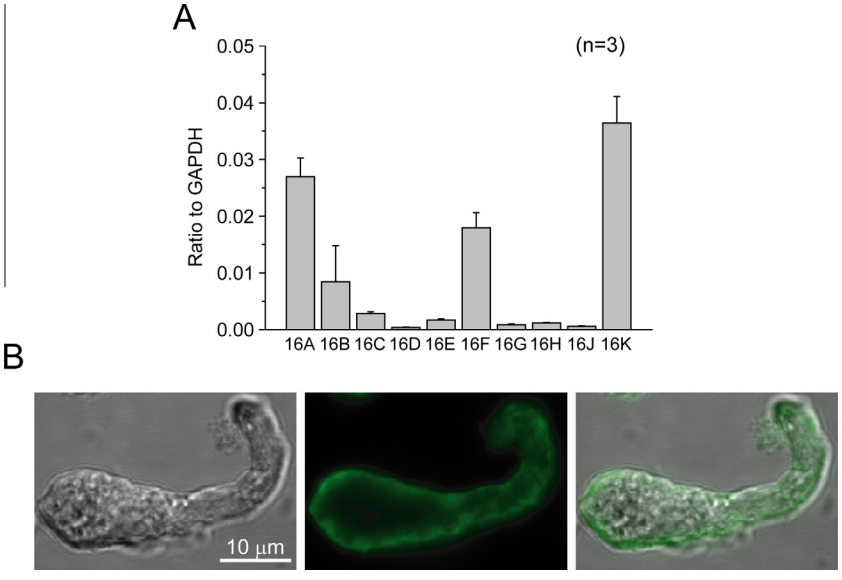

Fig. 1. (A) Quantitative PCR analysis of ten members of TMEM16 family in portal vein from male mice (n = 3 for each). Values are shown for steady state transcripts relative to GAPDH as an internal standard. (B) Immunofluorescence detection of TMEM16A on the plasma membrane of a mPVSMC using a laser scanning confocal microscope. Shown are transmitted light (*left*), fluorescence (*middle*), and merge (*right*) images, respectively. The bar represents 10 μm.

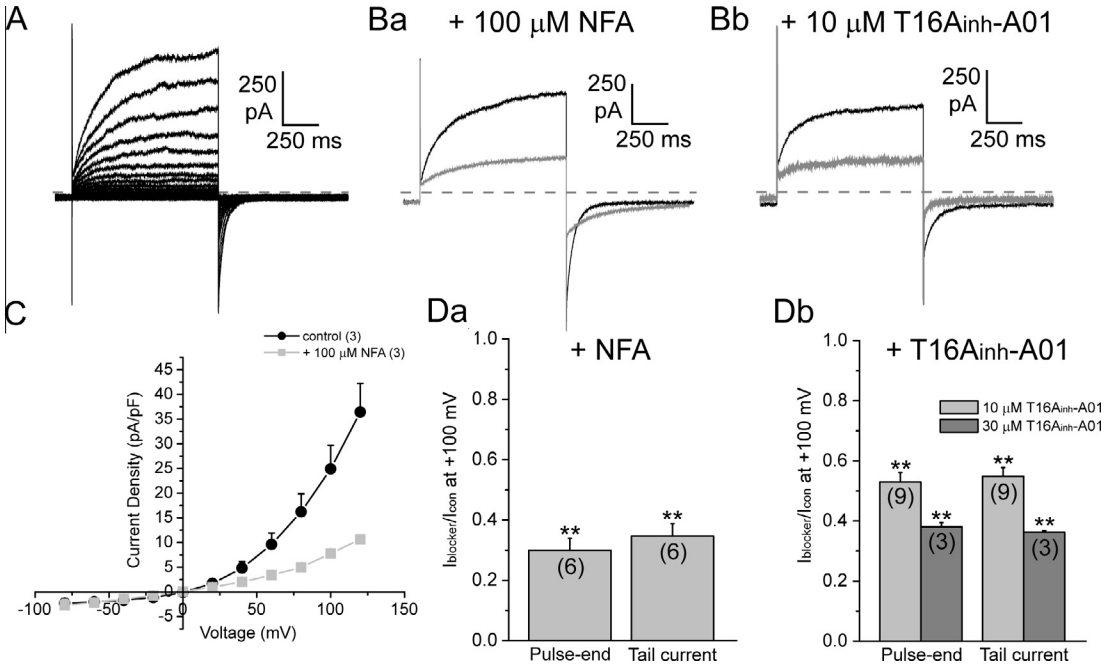

Fig. 2. (A) Representative CaCC currents in single mPVSMC under voltage-clamp. Test pulses were applied in 20-mV increments from −80 to +120 mV. CaCC currents exhibit time-dependent activation at positive membrane potentials. The dashed line indicates zero current level. (B) CaCC currents at +100 mV (*black*) were inhibited by applications of 100 μM niflumic acid (NFA) (*Ba, gray*) or 10 μM T16A$_{inh}$-A01 (*Bb, gray*), respectively. (C) Current density–voltage relationship measured at the end of the test pulses. The current reversed at near 0 mV, the theoretical equilibrium potential of Cl^-. (D) Summarized data for the effect of NFA (*Da*) or T16A$_{inh}$-A01 (*Db*) on pulse-end currents and followed inward tail currents. ** Statistical significance versus control at $P < 0.01$.

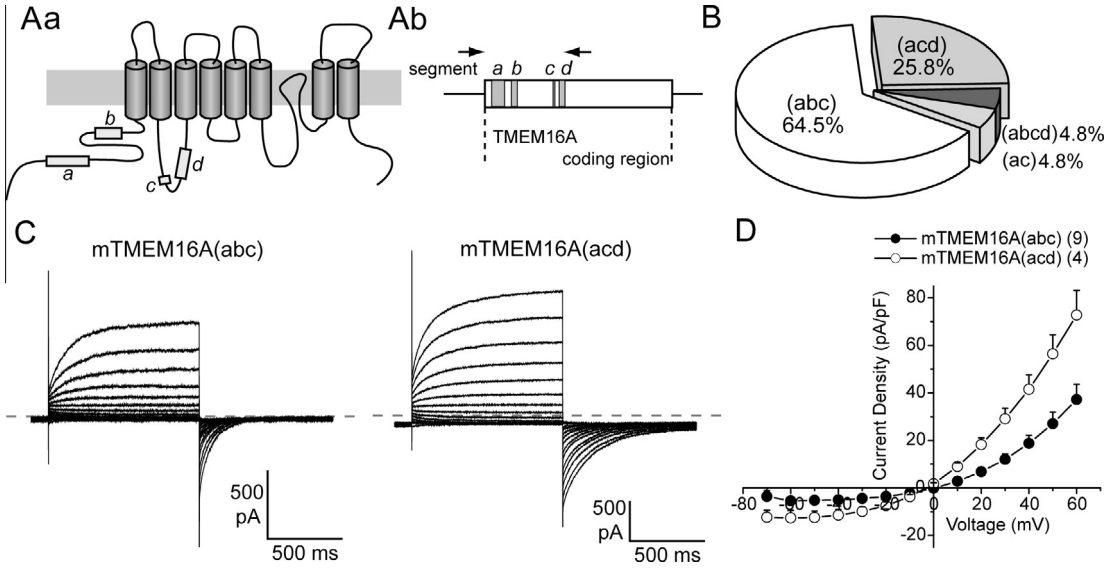

Fig. 3. (Aa) Putative topology of mouse TMEM16A according to mouse full-length TMEM16A (GenBank Accession No. NM_178642) and ref [11]. Four square boxes indicate alternatively spliced segments (segment *a–d*). (Ab) Schematic representation of TMEM16A mRNA. Arrows indicate primer set. (B) Quantification of the percentage of TMEM16A isoforms. 62 clones were obtained and analyzed with an ABI PRIZM 3130 genetic analyzer. (C) Representative CaCC currents in HEK293 cells expressing TMEM16A(*abc*) or TMEM16A(*acd*). Test pulses were applied in 10-mV increments from −70 to +60 mV. The dashed line indicates zero current level. (D) Current density–voltage relationships were measured at the end of the test pulses in HEK293 cells transiently expressing mTMEM16A(*abc*)(●) or mTMEM16A(*acd*)(○).

to confirm the nucleotide sequences, amplified PCR products were sequenced (Fig. 3Ab). It was found that two splicing variants, TMEM16A(*abc*) and TMEM16A(*acd*) were predominantly expressed in mPVSMCs (*abc*: 64.5%, *acd*: 25.8%, *abcd*: 4.8%, and *ac*: 4.8%, Fig. 3B, $n = 62$).

To confirm characteristic of the major spliced variants, the currents due to the activation of TMEM16A(*abc*) and TMEM16A(*acd*) were measured in HEK293 cells, where these variants were transiently expressed. The current shapes and current-voltage relationships of membrane currents upon depolarization were very similar to those CaCC currents in mPVSMCs (Fig. 3C and D). The deactivation kinetics of CaCC in mPVSMCs appears to be somewhat faster than those in two reconstituted TMEM16A currents. When the same amount of cDNAs were applied for transfection, the peak outward current density at +60 mV was 37.2 ± 6.4 pA/pF in mTMEM16A(*abc*) ($n = 9$) and 72.8 ± 10.3 pA/pF ($n = 4$) in mTMEM16A(*acd*),

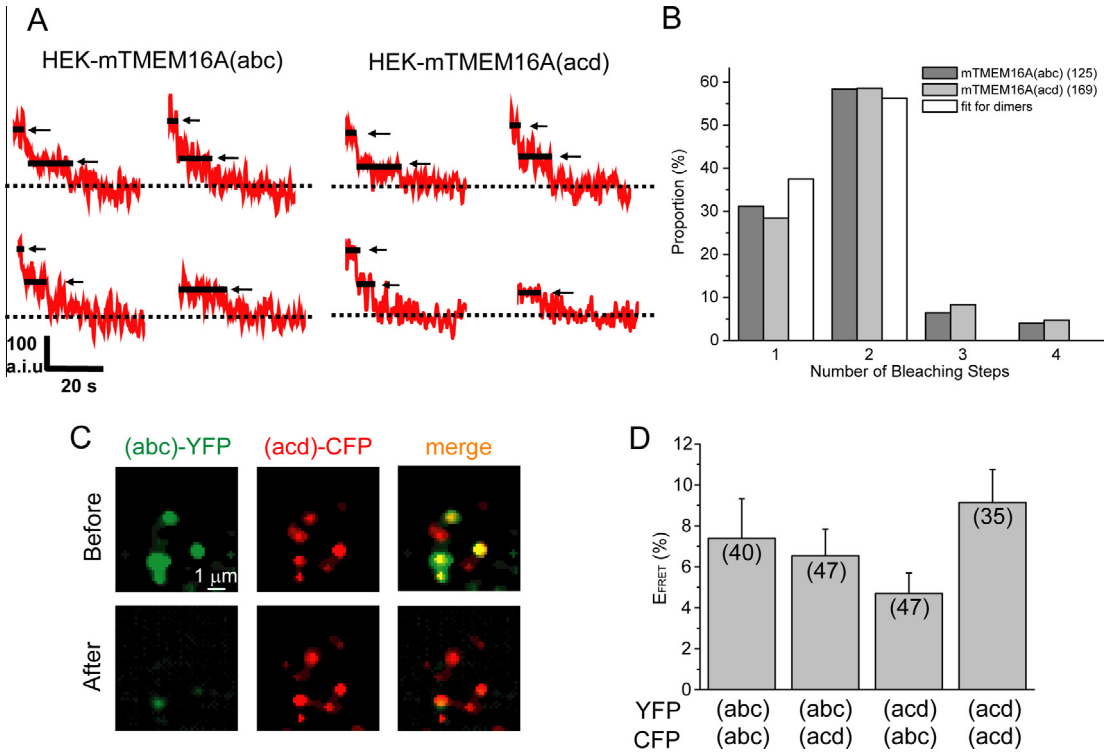

Fig. 4. (A) Representative intensity-time traces showing photobleaching steps observed in TMEM16A-GFP. Counting of the number of bleaching steps for TMEM16A(*abc*)-GFP or TMEM16A(*acd*)-GFP. The bleaching steps of GFP fluorescence in a TIRF region were counted for determining the number of TMEM16A-GFP oligomerizations within a single fluorescent particle based on the single-molecule photobleaching method. Arrows and solid line show bleaching step(s). Dotted line indicates complete bleaching level. (B) The number of bleaching steps in HEK293 cells expressing TMEM16A-GFP was summarized. The white bars indicate the binominal distribution expected for homodimers with a probability of 0.75 for a single GFP to be fluorescent. (C) TIRF images of HEK293 cells co-expressing TMEM16A(*abc*)-YFP and TMEM16A(*acd*)-CFP. Shown images were taken before (*top*) and after (*bottom*) TMEM16A(*abc*)-YFP bleaching. YFP and CFP fluorescence are indicated by green and red signals, respectively. The bar represents 1 μm. (D) FRET efficiencies (E_{FRET}) were summarized. The numbers of analyzed particles are shown in parentheses.

respectively (Fig. 3C and D). The deactivation time course of the tail currents in TMEM16A(*abc*) appeared to be faster than that in TMEM16A(*acd*), while not examined exactly in this study. Although the segment "*b*" is one of two putative calmodulin binding sites in TMEM16A, the sensitivity to intracellular Ca^{2+} concentration ($[Ca^{2+}]_i$) of TMEM16A(*ac*) is higher than TMEM16A(*abc*) [12]. The present results that larger current was observed in "*acd*" than "*abc*" may fit to the previous finding [12]. The mechanisms underlying the regulation of sensitivity to $[Ca^{2+}]_i$ in TMEM16A remains to be clarified.

3.4. TMEM16A isoforms can form dimers

As to the formation of CaCC, the domain in cytoplasmic N-terminus of TMEM16A is critical for homodimerization [28]. Since this region for dimerization does not overlap with the segments *a*–*d*, it can be possible that "heterodimer" as well as homodimer can be formed between different TMEM16A splicing variants. In the next series of experiments, we performed the single-molecule fluorescence bleaching analyses to determine the direct interaction between TMEM16A molecules in living cells.

First, TMEM16A(*abc*) labeled with GFP at C-terminus was expressed in HEK293 cells. When the GFP was photobleached, most fluorescent signals showed one or two step bleaching (1 step, 31.2%; 2 steps, 58.4%; 3 steps, 6.4%; 4 steps, 4.0%, 125 particles from 27 cells) (Fig. 4A and B). Similarly, in TMEM16A(*acd*)-GFP expressing HEK293 cells, the majority of the TMEM16A(*acd*)-GFP spots bleached in one or two steps (1 step, 28.4%; 2 steps, 58.6%; 3 steps, 8.3%; 4 steps, 4.7%, 169 particles from 31 cells). The method analyzing subunit number has been developed in the NMDA receptor subunits counting as membrane protein [17]. The resulting distribution of step numbers in this study fit well with a binomial distribution for homodimer, given that not all the GFP but only 75% of them emit fluorescent signal [17] (Fig. 4B, open bars). Three or four photobleaching steps observed in both cells are likely due to overlapping channels with in one region [17]. These results show for the first time in a living cell, to our knowledge, that TMEM16A molecules preferentially form dimers.

In the next part of this study, we examined the possibility that TMEM16A splicing variants can form heterodimers. To elucidate whether two TMEM16A isoforms directly interact each other to form heterodimer, FRET analyses were performed using TMEM16A(*abc*) and TMEM16A(*acd*) labeled with CFP or YFP, respectively. First, the co-localization of YFP and CFP signals were examined in HEK293 cells, in which CFP or YFP-labeled TMEM16A. The co-localization of *abc*-YFP and *abc*-CFP was 46.0%, that of *abc*-YFP and *acd*-CFP was 56.0% (Fig. 4C), that of *acd*-YFP and *abc*-CFP was 57.3%, and that of *acd*-YFP and *acd*-CFP was 57.4%. The increase in CFP fluorescence intensity was observed after YFP photobleaching. The E_{FRET} in cells expressing the same isoforms labeled with CFP or YFP was comparable to that in cells expressing different isoforms; $E_{FRET} = 7.4 \pm 1.9\%$ between *abc*-YFP and *abc*-CFP (40 particles from 11 cells), $E_{FRET} = 6.5 \pm 1.3\%$ between *abc*-YFP and *acd*-CFP (47 particles from 12 cells), $E_{FRET} = 4.7 \pm 1.0\%$ between *acd*-YFP and *abc*-CFP (47 particles from 10 cells), $E_{FRET} = 9.1 \pm 1.6\%$ between *acd*-YFP and *acd*-CFP (35 particles from 10 cells) (Fig. 4D). These results indicate that TMEM16A spliced variants can form dimers between different isoforms as well as the same ones.

In VSMCs, TMEM16A may regulate spontaneous activity, muscle tone and cell proliferation [6,7]. TMEM16A is abundantly expressed also in interstitial cells of Cajal (ICCs) in gastrointestinal tracts and contributes to normal motility via the initiation of electrical slow wave as the pacemaker potentials [29,30]. ICC-like cells

were isolated from rabbit portal vein and exhibit rhythmical intracellular Ca^{2+} oscillations or spontaneous transient inward currents (STICs) similar to ICCs [31,32]. Besides, it has been speculated that TMEM16A splicing variants may differentially contribute to CaCC activity. Skipping translation of segment *b* and *d* have been reported in various tissues and considered to alter electrophysiological properties of TMEM16A such as Ca^{2+} sensitivity and kinetics [12,14]. Multiple transcripts of TMEM16A have been identified, though their detail properties have not been clear yet. It has been reported that the expression level of TMEM16A splicing variants are altered in patients with diabetic gastroparesis [14].

In conclusion, TMEM16A splicing variants, supposed to be mainly *abc* and *acd*, contribute to CaCC activity in mPVSMCs and the characteristics of CaCC are presumably determined by the multiple combinations of hetero-/homo-dimers of variant isoforms. The combination of alternative splicing patterns may play obligatory roles in diverse physiological functions and the changes in combination patterns may possibly be responsible for pathological phenomena.

Acknowledgments

This investigation was supported by a Grant-in-Aid for Scientific Research on Priority Areas from the Ministry of Education, Culture, Sports, Science, and Technology (23136512 and 25136717; to Y.I.) and Grant-in-Aids for Scientific Research (B) (23390020; to Y.I.) from the Japan Society for the Promotion of Science.

References

[1] K. Kitamura, J. Yamazaki, Chloride channels and their functional roles in smooth muscle tone in the vasculature, Jpn. J. Pharmacol. 85 (2001) 351–357.
[2] S.N. Saleh, I.A. Greenwood, Activation of chloride currents in murine portal vein smooth muscle cells by membrane depolarization involves intracellular calcium release, Am. J. Physiol. Cell Physiol. 288 (2005) C122–131.
[3] A. Caputo, E. Caci, L. Ferrera, N. Pedemonte, C. Barsanti, E. Sondo, U. Pfeffer, R. Ravazzolo, O. Zegarra-Moran, L.J. Galietta, TMEM16A, a membrane protein associated with calcium-dependent chloride channel activity, Science 322 (2008) 590–594.
[4] B.C. Schroeder, T. Cheng, Y.N. Jan, L.Y. Jan, Expression cloning of TMEM16A as a calcium-activated chloride channel subunit, Cell 134 (2008) 1019–1029.
[5] Y.D. Yang, H. Cho, J.Y. Koo, M.H. Tak, Y. Cho, W.S. Shim, S.P. Park, J. Lee, B. Lee, B.M. Kim, R. Raouf, Y.K. Shin, U. Oh, TMEM16A confers receptor-activated calcium-dependent chloride conductance, Nature 455 (2008) 1210–1215.
[6] H. Sun, Y. Xia, O. Paudel, X.R. Yang, J.S. Sham, Chronic hypoxia-induced upregulation of Ca^{2+}-activated Cl^- channel in pulmonary arterial myocytes: a mechanism contributing to enhanced vasoreactivity, J. Physiol. 590 (2012) 3507–3521.
[7] S. Bulley, Z.P. Neeb, S.K. Burris, J.P. Bannister, C.M. Thomas-Gatewood, W. Jangsangthong, J.H. Jaggar, TMEM16A/ANO1 channels contribute to the myogenic response in cerebral arteries, Circ. Res. 111 (2012) 1027–1036.
[8] A.J. Davis, J. Shi, H.A. Pritchard, P.S. Chadha, N. Leblanc, G. Vasilikostas, Z. Yao, A.S. Verkman, A.P. Albert, I.A. Greenwood, Potent vasorelaxant activity of the TMEM16A inhibitor $T16A_{inh}$-A01, Br. J. Pharmacol. 168 (2013) 773–784.
[9] A.J. Davis, A.S. Forrest, T.A. Jepps, M.L. Valencik, M. Wiwchar, C.A. Singer, W.R. Sones, I.A. Greenwood, N. Leblanc, Expression profile and protein translation of TMEM16A in murine smooth muscle, Am. J. Physiol. Cell Physiol. 299 (2010) C948–959.
[10] G. Fallah, T. Romer, S. Detro-Dassen, U. Braam, F. Markwardt, G. Schmalzing, TMEM16A(a)/anoctamin-1 shares a homodimeric architecture with CLC chloride channels, Mol. Cell. Proteomics 10 (2011) 1–10.
[11] K. Yu, C. Duran, Z. Qu, Y.Y. Cui, H.C. Hartzell, Explaining calcium-dependent gating of anoctamin-1 chloride channels requires a revised topology, Circ. Res. 110 (2012) 990–999.
[12] L. Ferrera, A. Caputo, I. Ubby, E. Bussani, O. Zegarra-Moran, R. Ravazzolo, F. Pagani, L.J. Galietta, Regulation of TMEM16A chloride channel properties by alternative splicing, J. Biol. Chem. 284 (2009) 33360–33368.
[13] Y. Tian, P. Kongsuphol, M. Hug, J. Ousingsawat, R. Witzgall, R. Schreiber, K. Kunzelmann, Calmodulin-dependent activation of the epithelial calcium-dependent chloride channel TMEM16A, FASEB J. 25 (2011) 1058–1068.
[14] A. Mazzone, C.E. Bernard, P.R. Strege, A. Beyder, L.J. Galietta, P.J. Pasricha, J.L. Rae, H.P. Parkman, D.R. Linden, J.H. Szurszewski, T. Ördög, S.J. Gibbons, G. Farrugia, Altered expression of Ano1 variants in human diabetic gastroparesis, J. Biol. Chem. 286 (2011) 13393–13403.
[15] H. Yamamura, C. Ikeda, Y. Suzuki, S. Ohya, Y. Imaizumi, Molecular assembly and dynamics of fluorescent protein-tagged single $K_{Ca}1.1$ channel in expression system and vascular smooth muscle cells, Am. J. Physiol. Cell Physiol. 302 (2012) C1257–1268.
[16] Y. Imaizumi, K. Muraki, M. Watanabe, Ionic currents in single smooth muscle cells from the ureter of the guinea-pig, J. Physiol. 411 (1989) 131–159.
[17] M.H. Ulbrich, E.Y. Isacoff, Subunit counting in membrane-bound proteins, Nat. Methods 4 (2007) 319–321.
[18] F.C. Britton, S. Ohya, B. Horowitz, I.A. Greenwood, Comparison of the properties of *CLCA1* generated currents and $I_{Cl(Ca)}$ in murine portal vein smooth muscle cells, J. Physiol. 539 (2002) 107–117.
[19] V.V. Matchkov, P. Larsen, E.V. Bouzinova, A. Rojek, D.M. Boedtkjer, V. Golubinskaya, F.S. Pedersen, C. Aalkjaer, H. Nilsson, Bestrophin-3 (vitelliform macular dystrophy 2-like 3 protein) is essential for the cGMP-dependent calcium-activated chloride conductance in vascular smooth muscle cells, Circ. Res. 103 (2008) 864–872.
[20] B. Manoury, A. Tamuleviciute, P. Tammaro, TMEM16A/anoctamin 1 protein mediates calcium-activated chloride currents in pulmonary arterial smooth muscle cells, J. Physiol. 588 (2010) 2305–2314.
[21] C. Thomas-Gatewood, Z.P. Neeb, S. Bulley, A. Adebiyi, J.P. Bannister, M.D. Leo, J.H. Jaggar, TMEM16A channels generate Ca^{2+}-activated Cl^- currents in cerebral artery smooth muscle cells, Am. J. Physiol. Heart Circ. Physiol. 301 (2011) H1819–1827.
[22] H. Yang, A. Kim, T. David, D. Palmer, T. Jin, J. Tien, F. Huang, T. Cheng, S.R. Coughlin, Y.N. Jan, L.Y. Jan, TMEM16F forms a Ca^{2+}-activated cation channel required for lipid scrambling in platelets during blood coagulation, Cell 151 (2012) 111–122.
[23] J.R. Martins, D. Faria, P. Kongsuphol, B. Reisch, R. Schreiber, K. Kunzelmann, Anoctamin 6 is an essential component of the outwardly rectifying chloride channel, Proc. Natl. Acad. Sci. USA 108 (2011) 18168–18172.
[24] S. Grubb, K.A. Poulsen, C.A. Juul, T. Kyed, T.K. Klausen, E.H. Larsen, E.K. Hoffmann, TMEM16F (Anoctamin 6), an anion channel of delayed Ca^{2+} activation, J. Gen. Physiol. 141 (2013) 585–600.
[25] T. Shimizu, T. Iehara, K. Sato, T. Fujii, H. Sakai, Y. Okada, TMEM16F is a component of a Ca^{2+}-activated Cl^- channel but not a volume-sensitive outwardly rectifying Cl^- channel, Am. J. Physiol. Cell Physiol. 304 (2013) C748–759.
[26] W. Namkung, P.W. Phuan, A.S. Verkman, TMEM16A inhibitors reveal TMEM16A as a minor component of calcium-activated chloride channel conductance in airway and intestinal epithelial cells, J. Biol. Chem. 286 (2011) 2365–2374.
[27] V. Cenedese, G. Betto, F. Celsi, O.L. Cherian, S. Pifferi, A. Menini, The voltage dependence of the TMEM16B/anoctamin2 calcium-activated chloride channel is modified by mutations in the first putative intracellular loop, J. Gen. Physiol. 139 (2012) 285–294.
[28] J. Tien, H.Y. Lee, D.L. Minor Jr., Y.N. Jan, L.Y. Jan, Identification of a dimerization domain in the TMEM16A calcium-activated chloride channel (CaCC), Proc. Natl. Acad. Sci. USA 110 (2013) 6352–6357.
[29] S.J. Hwang, P.J. Blair, F.C. Britton, K.E. O'Driscoll, G. Hennig, Y.R. Bayguinov, J.R. Rock, B.D. Harfe, K.M. Sanders, S.M. Ward, Expression of anoctamin 1/TMEM16A by interstitial cells of Cajal is fundamental for slow wave activity in gastrointestinal muscles, J. Physiol. 587 (2009) 4887–4904.
[30] P.J. Gomez-Pinilla, S.J. Gibbons, M.R. Bardsley, A. Lorincz, M.J. Pozo, P.J. Pasricha, M. Van de Rijn, R.B. West, M.G. Sarr, M.L. Kendrick, R.R. Cima, E.J. Dozois, D.W. Larson, T. Ordog, G. Farrugia, Ano1 is a selective marker of interstitial cells of Cajal in the human and mouse gastrointestinal tract, Am. J. Physiol. Gastrointest. Liver Physiol. 296 (2009) G1370–1381.
[31] X. Huang, D. Zhao, Z.Y. Wang, M.L. Zhang, Z.Q. Yan, Y.F. Han, W.X. Xu, Z.L. Jiang, The properties of spontaneous transient inward currents of interstitial cells in rabbit portal vein, Eur. J. Pharmacol. 643 (2010) 63–69.
[32] M.I. Harhun, D.V. Gordienko, O.V. Povstyan, R.F. Moss, T.B. Bolton, Function of interstitial cells of Cajal in the rabbit portal vein, Circ. Res. 95 (2004) 619–626.